# Construction of anthropomorphic hybrid, dual-lattice voxel models for optimizing image quality and dose in radiography

Nina Petoussi-Henss\*, Janine Becker, Matthias Greiter, Helmut Schlattl, Maria Zankl,
Christoph Hoeschen
Research Unit Medical Radiation Physics and Diagnostics, Helmholtz Zentrum München,
Ingolstaedter Landstraße 1, 85764 Neuherberg, Germany

#### **ABSTRACT**

In radiography there is generally a conflict between the best image quality and the lowest possible patient dose. A proven method of dosimetry is the simulation of radiation transport in virtual human models (i.e. phantoms). However, while the resolution of these voxel models is adequate for most dosimetric purposes, they cannot provide the required organ fine structures necessary for the assessment of the imaging quality.

The aim of this work is to develop hybrid/dual-lattice voxel models (called also phantoms) as well as simulation methods by which patient dose and image quality for typical radiographic procedures can be determined. The results will provide a basis to investigate by means of simulations the relationships between patient dose and image quality for various imaging parameters and develop methods for their optimization.

A hybrid model, based on NURBS (Non Linear Uniform Rational B-Spline) and PM (Polygon Mesh) surfaces, was constructed from an existing voxel model of a female patient. The organs of the hybrid model can be then scaled and deformed in a non-uniform way i.e. organ by organ; they can be, thus, adapted to patient characteristics without losing their anatomical realism. Furthermore, the left lobe of the lung was substituted by a high resolution lung voxel model, resulting in a dual-lattice geometry model. "Dual lattice" means in this context the combination of voxel models with different resolution.

Monte Carlo simulations of radiographic imaging were performed with the code EGS4nrc, modified such as to perform dual lattice transport. Results are presented for a thorax examination.

**Keywords:** Voxel dual lattice model, phantom, image simulation, Monte Carlo

## 1. INTRODUCTION

Computational phantoms or models have been used up to now mostly for numerical dosimetry. At present, there exist three different types of computational anatomic phantoms: stylized (or mathematical), voxel (or tomographic), and hybrid types based upon NURBS and/or polygon mesh surfaces. The characteristics and advantages of each type of phantoms have been reviewed by Bolch et al<sup>1</sup>. Stylized phantoms have been used in radiation dosimetry for over 40 years<sup>2</sup>. They are composed of 3D geometric surface equations defining both internal organs and outer body surfaces. While they are flexible in terms of allowing changes in organ size, body shape, and extremity positioning, they are generally insufficient with respect to anatomic realism. Voxel phantoms, in contrast, are composed of a three dimensional array of voxels, each with a unique organ identity, elemental composition, and density. Voxel phantoms are assembled through segmentation of individual image slices from CT, MR or other image data, and thus they provide a high level of anatomic realism<sup>3, 4, 5</sup>. Their main limitations are that their construction is time-consuming and their inflexibility of adjustment to match individuals other than the person providing the source data. The third generation of phantoms is the so called hybrid type; the organs are described by either non-uniform rational B-spline (NURBS) or polygon mesh (PM) surfaces<sup>6, 7, 8</sup>. This offers both flexibility in organ alterations and anatomical realism. While most of

\*petoussi@helmholtz-muenchen.de; phone +49 89 31872791; +49 89 31872517

Medical Imaging 2014: Physics of Medical Imaging, edited by Bruce R. Whiting, Christoph Hoeschen, Despina Kontos, Proc. of SPIE Vol. 9033, 90331W ⋅ © 2014 SPIE ⋅ CCC code: 1605-7422/14/\$18 ⋅ doi: 10.1117/12.2043437

the hybrid phantoms were applied for dosimetry, Segars et al <sup>9</sup> generated 58 adult highly detailed 4D extended cardiactorso (XCAT) phantoms based on patient CT data to be used for imaging research.

The Research Unit Medical Radiation Physics and Diagnostics (AMSD) of the Helmholtz Zentrum München has been involved since over three decades in the evolution of anthropomorphic computational phantoms. Besides 2 mathematical phantoms<sup>10</sup>, 13 individual-based voxel phantoms<sup>11,3</sup> and 2 reference adult voxel phantoms (the latter in cooperation with ICRP)<sup>4</sup>, the group is developing dual lattice voxel models, combining high and lower resolution partial body voxel models.

Since the main purpose of existing models is the computation of organ/tissue doses for ionizing radiation or electromagnetic fields, their resolution is generally in the order of a few mm. Thus, they are not suited to simulate realistic images. Since whole-body high-resolution human models can hardly be obtained due to radiation dose constraints and would anyhow be difficult to be handled numerically, dual lattice voxel models, i.e., combined high and lower resolution voxel models, appear to be favorable. Depending on the diagnostic purpose, high-resolution models of certain organs are incorporated into these patient models. In order to verify that this method is applicable, in a first step, Monte Carlo simulations of a thorax radiography using a high-resolution lung model were performed.

## 2. METHODS

## 2.1. The whole body voxel model Laura and its NURBS version

For this work, the whole body voxel model "Laura" of an adult female, previously developed at AMSD, has been employed. Laura was constructed from computed tomographic (CT) image data of a 43 year old female patient. With 1.68 m height and 59 kg weight, the patient was close to the so-called reference female (1.63 kg and 60 kg)<sup>12</sup>. The voxel in-plane resolution was 1.875 mm and the slice thickness 5 mm, corresponding to a voxel volume of 17.6 mm<sup>3</sup> and ca. 2.6 million of voxels. A total of 88 tissues were primarily segmented in Laura. Figure 1a shows three dimensional representations of some of the organs of this model. More details about this phantom can be found at Zankl et al <sup>3</sup>.

As the first results of the simulated images have showed (see section 3), the original resolution of Laura was not sufficient for our purposes, so that the model had to be transformed to a NURBS/PM - based hybrid model. The method of construction of NURBS-based models was described, among others, by Lee et al 7. For the present work, the procedure of this transformation commences with the polygonization of the initial voxel model by rendering each organ separately a polygon mesh surface. using the software (http://www.exelisvis.com/ProductsServices/IDL.aspx). The rendering process resulted in jagged-looking objects which had to be smoothed. The PM data were therefore exported to the 3D modeling software, Rhinoceros (version 4.0) (Robert Mc Neel and Associates, USA). Subsequently, NURBS smooth surfaces were created for each organ. An exception of this procedure was the skeleton: the one used for this work was obtained as a PM surface from http://www.creativecrash.com/marketplace/3d-models/anatomy/skeletal-system/c/anatomy-skeleton-male. The contours of this skeleton were smooth, thus, it was not necessary to convert the PM to NURBS but its size and form were adjusted to fit the anatomy of the female model Laura.

Since the to-date Monte Carlo radiation transport codes cannot be coupled to NURBS or PM surface geometries, the resulting NURBS and PM organs have then been re-voxelized. This was achieved by triangulation with Rhinoceros and then by voxelization with the software Binvox <a href="http://www.cs.princeton.edu/~min/binvox/">http://www.cs.princeton.edu/~min/binvox/</a>). For memory purposes, a resolution of 500 microns was chosen for the revoxelization of the NURBS/PM model. Figure 1 (b) and 2 show examples of the procedure.

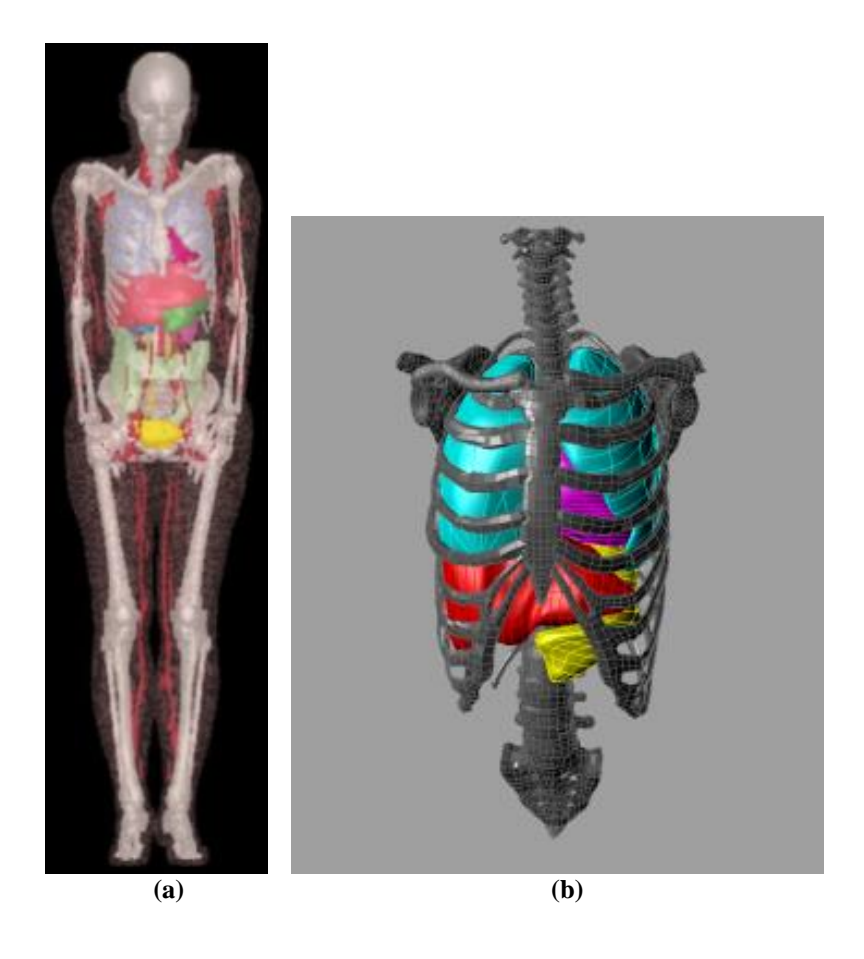


Figure 1. The whole-body voxel phantom Laura (a). Lungs, stomach, heart and liver of the phantom as NURBS surfaces and the skeleton as PM surface (b).

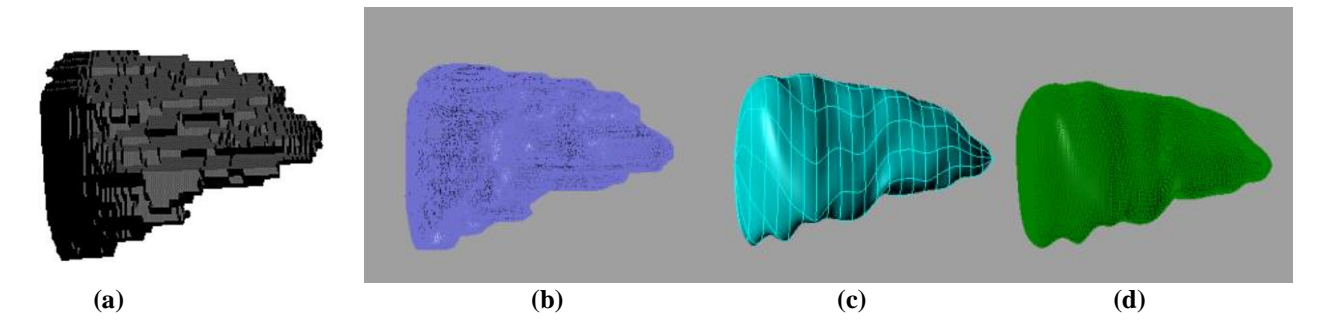


Figure 2. Rendered images of the liver as an example of the process: original voxel model of the liver (a), corresponding polygon mesh (b), its NURBS surface model (c), polygon mesh model from NURBS (d).

# 2.2. The high resolution model of the lung

To construct the high resolution model of a lung, a lung specimen<sup>13</sup> was scanned by a GE/phoenix|x-ray cone-beam CT "v|tome|x" (http://www.ge-mcs.com/en/phoenix-xray.html) at a resolution of 114 microns, resulting in 3000 slices. The lung was dry and fixed in gas-filled state. Because of the large density difference between gas and tissue, a good distinction between the tissue, the interior of the airways and alveoles could be achieved. This procedure presented several challenges: due to technical restrictions of the image device, the specimen had to be scanned in three distinct operations and the resulting image data sets were then re-assembled together. The volume of the CT data was reduced from originally 22 to 6.6 GB. The phantom of the whole lung consists of ca. 4.5 billion voxels of (0.11 mm)<sup>3</sup> dimension.

Since proper segmentation of the different lung structures was not possible due to the complexity of the data, the non-calibrated gray values were related to their attenuation coefficients. For this purpose, the lung was scanned in addition in a standard medical CT (GE Brightspeed 16) (<a href="http://www.ge-mcs.com/de/radiography-x-ray/ct-computed-tomography.html">http://www.ge-mcs.com/de/radiography-x-ray/ct-computed-tomography.html</a>) to obtain calibrated pixel values. The uncalibrated numbers of the high-resolution scan were then converted into Hounsfield units (HU) by scaling the gray values, so that its histogram was similar to that of the low-resolution lung. Since a real lung, in contrast to the specimen, contains a considerable amount of blood and other fluids, the gray values had to be further scaled. For this purpose, the CT scan of the patient whose image data were utilized to construct the model Laura has been used. However, the fitting of the histogram of the high-resolution lung to the respective one of the patient is not yet optimal and would be improved in the future.

Finally, the resulting HU values were binned into 27 different intervals. These were then assigned to either lung parenchyma (HU < 0), cartilage (0 < HU < 1000) or mineral bone (1000 < HU < 3000) with elemental compositions according to ICRP Publication 89<sup>12</sup>. The densities were adjusted to reproduce the HU values in each bin for the x-ray spectrum used in the imaging of the lung specimen.

As a cross-check for the different gray value scaling and assignment to a medium, the mass of the lung model was determined: the model of the "dry" lung resulted to a mass of about 200g, while the mass of the actual lung specimen was 216g. The mass of the model of the lung including blood and other fluids was 540g, which is about 10% heavier than the left lung of Laura with its 500g. Thus, the composition of the high resolution lung model is considered to provide a realistic representation of the composition of the human lung.

## 2.3. Monte Carlo simulations

The particle transport inside the hybrid phantom has been simulated with the Monte Carlo code EGSnrc<sup>14</sup>. Due to the combination of the high and low resolution organs, the code has been modified to perform dual lattice transport. The model consists of a three-dimensional voxel matrix, wherein each voxel is assigned a unique medium. The Monte Carlo code follows a particle through the body until it hits the image detector. Transmission, absorption and scattering of the photons through the virtual phantom were simulated. In this way, the organ doses can be calculated as well as projection images can be modeled.

With the hybrid/dual-lattice model described in the previous section, a thorax posterior examination was simulated. Firstly, a test calculation was performed where only a portion of the entire high resolution lung model has been used and embedded in Laura. The tube voltage was 75 kV and the filtration 2 mm aluminum. The focus-to-detector distance was 75 cm and the detector was 15 cm in front of the model. The detector was composed from  $900 \times 800$  pixels with a pixel size of  $500 \times 500 \ \mu m^2$ . In the simulation, 24 billion photons were followed.

For a further, more realistic simulation, the entire lung model was embedded in the whole body model Laura; tube voltage was taken to be of 110 kV and filtration 2.5 mm Al, typical values for thorax radiographs. The focus-to-detector distance was now 115 cm, and the detector was  $\approx$ 10 cm in front of the model. The detector had  $1000 \times 1800$  pixels with a pixel size of  $144 \times 144 \ \mu m^2$ . For this simulation, 100 billion photons were followed.

For comparison purposes, and for both cases stated above, simulations were also performed for the high resolution model of the lung standing on its own, i.e. not embedded in the whole phantom. To achieve similar noise levels as in the simulations before, the numbers of histories have been reduced to 4 and 17 billion, respectively.

# 3. RESULTS

As explained above, for the initial simulation test, only a portion of the entire model has been used. The high-resolution model of the lung was fitted into the original version of the model Laura, where first the original resolution (see 2.1) of Laura was retained. The resulting image of a first test simulation for a thorax radiograph with 75 kV is shown in the right panel of Figure 3. The low resolution of the original Laura model results in jagged, step structures, particularly at the edges of the ribs in the simulated x-ray image (a). These steps eventually cover the fine structures which are present in the high-resolution lung model alone (b) preventing therefore their recognition.

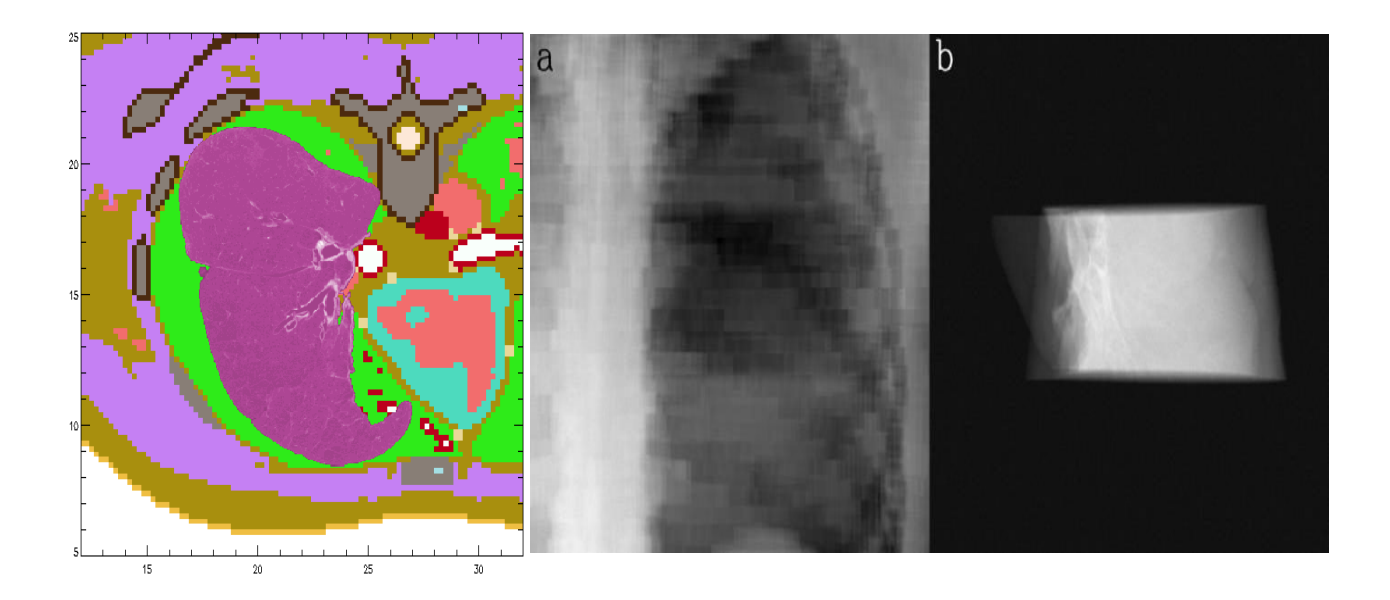


Figure 3. Transverse slice of the voxel model with embedded high-resolution lung (far left); simulated lung examination with the high-resolution partial model of the lung (a) and simulated examination of the lung without the body model (b). It can be seen that the voxels having low resolution appear as large steps and prohibit the visualization of the fine structures.

For this reason it was necessary to smooth also the edges of the organs in the body model surrounding the high-resolution organ model. This was achieved by creating a NURBS/PM-based representation of the body model as described above. The left panel of Figure 4 shows a slice of the NURBS/PM model combined with the high-resolution lung model. In the right panel, simulated images (a) of the combined model and (b) of the bare high resolution lung are shown with similar gray value windowing. It can be seen, that the spine and ribs are now clearly visible and the fine structure of the lung is easily recognizable.

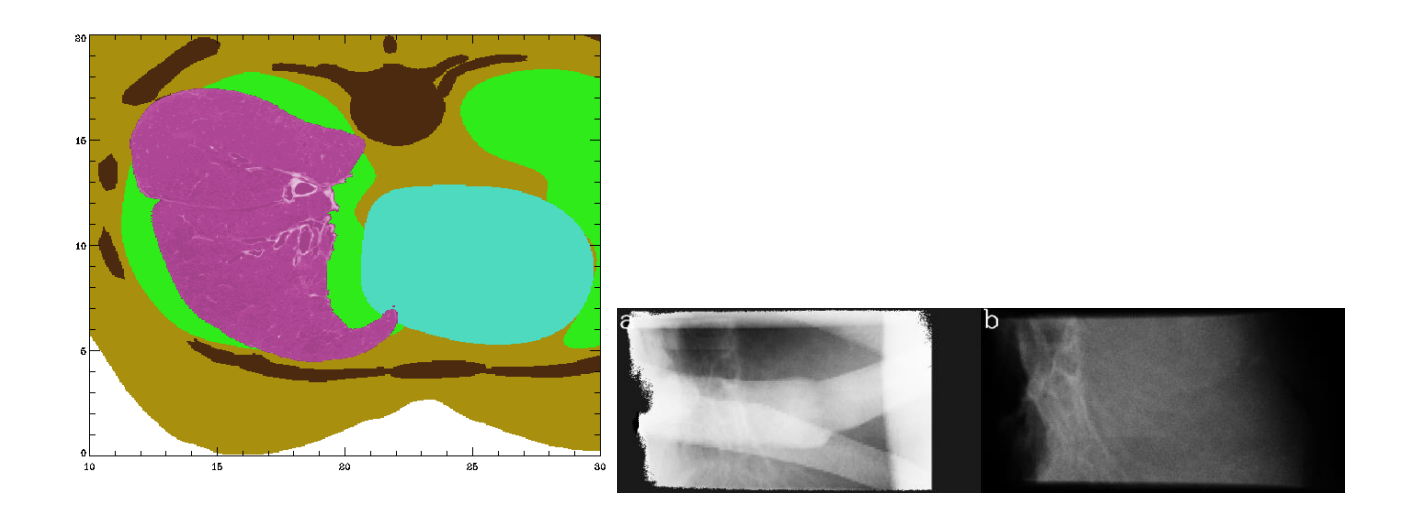


Figure 4. Transverse slice of the "smoothed" voxel model with embedded high-resolution lung (left); Simulated lung examination with a high-resolution partial model of the lung in the smoothed via NURBS body model (a) and simulated examination of the lung without body model (b).

Figure 5a shows the simulation of the image when the complete left lung is embedded in the phantom, for tube voltage of 110 kV. The fine structures of the lung specimen (Figure. 5b) are recognizable in almost the whole image. This becomes more apparent when only small areas are considered and the gray values are windowed appropriately. As an example, in Figure 6, a small region near the center of the image of Figure 5 is enlarged and the gray values adjusted. It can be seen that all details visible in the green box of Figure 6b can also be detected in Figure 6a. Thus, the influence of various technical examination parameters on the resulting image quality measures e.g., contrast-to-noise ratio, MTF or NPS can be investigated with this hybrid/dual-lattice model.

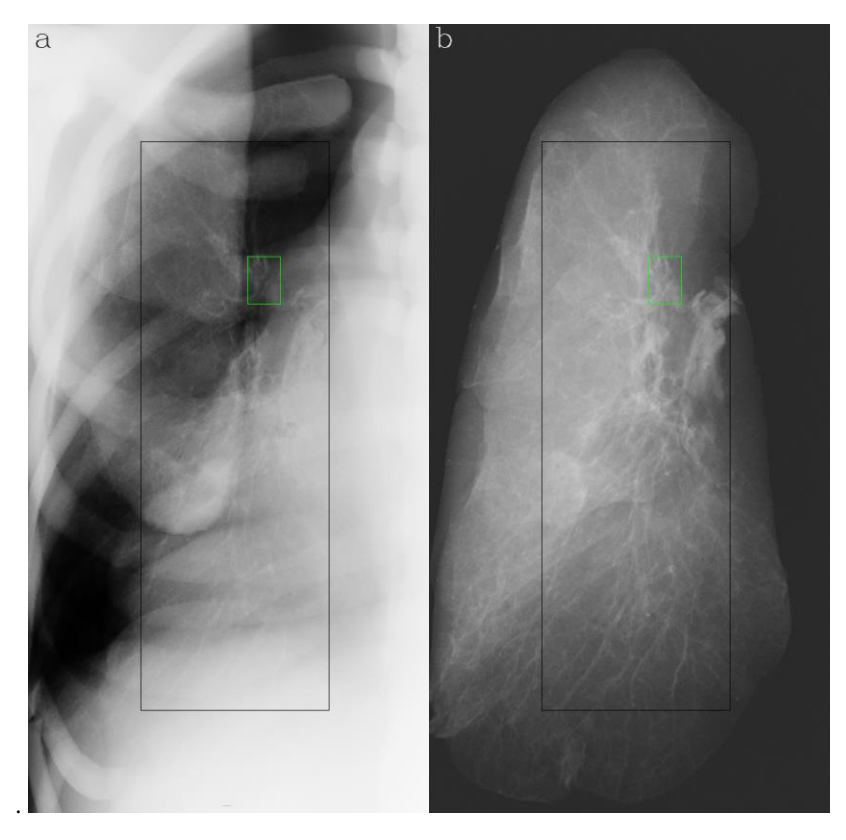


Figure 5. Simulation of a lung examination with embedded high-resolution lung in the NURBS body model (a); for comparison, the lung without the body model is shown in (b). The gray scale is adjusted to show the full contrast range on the region of interest (black box). The region marked by the smaller box in green is shown in Figure 6.

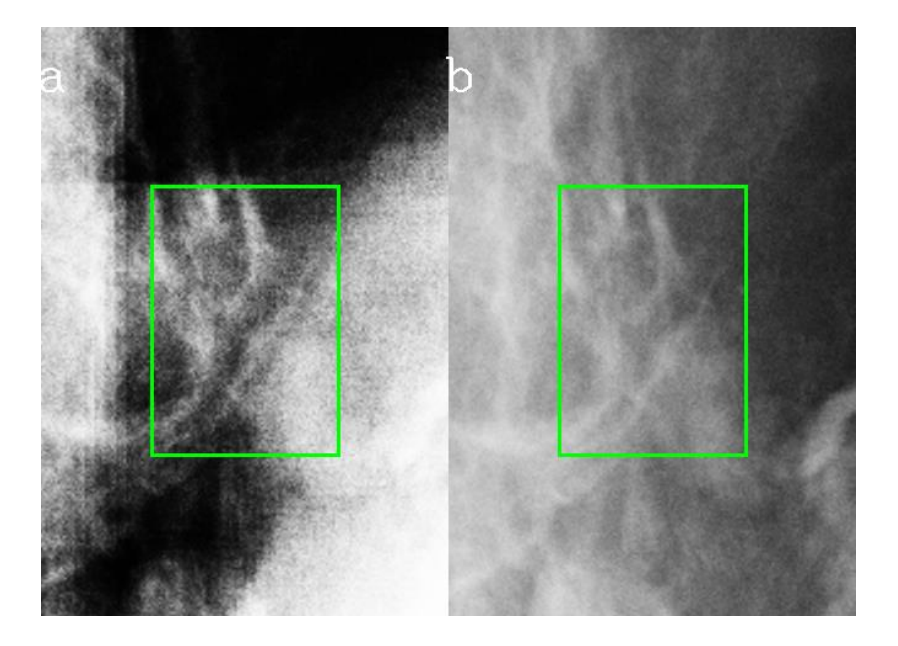


Figure 6. Enlarged region of Figure 5 showing fine structures of the high-resolution lung model (a: embedded in NURBS body model, b: solely lung).

## 4. CONCLUSION

A NURBS/PM model was created from a whole body voxel model. This type of model allows easy modification of anatomical attributes as well as posture and it can be re-voxelised to any resolution. Furthermore, a high resolution voxel model of a lung has been developed. It was shown that voxel models of different voxel resolution can be combined – higher resolution in partial body (for example, lung or breast) and lower resolution in the rest of the body. An image simulation for a lung posterior-anterior examination was performed. The left lung could be clearly seen in the simulated image, together with finer structures. Thus, the basis to investigate the influence of patient stature and technical examination parameters, such as tube voltage, filtration, and focus-to-detector distance, on various image quality measures (e.g., contrast-to-noise ratio, MTF or NPS) by simulations has been established.

## REFERENCES

- [1] Bolch, W., Lee, C., Wayson, M. and Johnson, P., "Hybrid computational phantoms for medical dose reconstruction," Radiat. Environ. Biophys. 49, 155-168 (2010).
- [2] Eckerman, K. E., Poston, J. W., Bolch, W. E. and Xu, X. G., Stylized Computational Phantoms Developed at ORNL and Elsewhere, Taylor & Francis, Boca Raton, London, New York (2010).
- [3] Zankl, M., The GSF voxel computational phantom family, Taylor & Francis, Boca Raton, London, New York (2010).
- [4] ICRP, *Adult reference computational phantoms*, ICRP Publication 110, International Commission on Radiological Protection, Oxford, UK (2009).
- [5] Habib, Z. and Xie, X. G., "Computational Anthropomorphic Models of the Human Anatomy: The Path to Realistic Monte Carlo Modeling in Radiological Sciences," Annual Review of Biomedical Egineering 9, 471-500 (2007).
- [6] Lee, C., Lee, C., Lodwick, D. and Bolch, W. E., "NURBS-based 3-D anthropomorphic computational phantoms for radiation dosimetry applications," Radiat. Prot. Dosim. 127, 227-232 (2007).
- [7] Lee, C., Lodwick, D., Hurtado, J., Pafundi, D., Lwilliams, J. and Bolch, W. E., "The UF family of reference hybrid phantoms for computational radiation dosimetry," Phys. Med. Biol. 55, 339-363 (2010).
- [8] Kim, C. H., Jeong, J. H., Bolch, W. E., Cho, K.-W. and Hwang, S. B., "A polygon-surface reference Korean male phantom (PSRK-Man) and its direct implementation in Geant4 Monte Carlo simulation," Phys. Med. Biol. 56, 3137 (2011).
- [9] W. P. Segars, J. B., J. Frush, S. Hon, C. Eckersley, C. H. Williams, J. Feng, D. J. Tward, J. T. Ratnanather, M. I. Miller, D. Frush, E. Samei, "Population of anatomically variable 4D XCAT adult phantoms for imaging research and optimization," Med. Phys. 40, 11 (2013).
- [10] Kramer, R., Zankl, M., Williams, G. and Drexler, G., *The calculation of dose from external photon exposures using reference human phantoms and Monte Carlo methods, Part I: The male (Adam) and female (Eva) adult mathematical phantoms*, GSF-Report S-885, GSF National Research Center for Environment and Health, Neuherberg, Germany (1982).
- [11] Petoussi-Henss, N., Zankl, M., Fill, U. and Regulla, D., "The GSF family of voxel phantoms," Phys. Med. Biol. 47, 89-106 (2002).
- [12] ICRP, Basic anatomical and physiological data for use in radiological protection: reference values, ICRP Publication 89, Pergamon Press, Oxford, UK (2002).
- [13] Hoeschen, C., Buhr, E. and Döhring, W., "High-spatial-resolution measurement of x-ray intensity pattern in a radiograph of the thorax," Proc. SPIE Medical Imaging 3659, 432-443 (1999).
- [14] Kawrakow, I., Mainegra-Hing, E., Rogers, D. W. O., Tessier, F. and Walters, B. R. B., *The EGSnrc code system: Monte Carlo simulation of electron and photon transport*, PIRS Report 701, National Research Council of Canada (NRCC), Ottawa (2009).